ADVANCED MATERIALS
www.advmat.de

An Active Metamaterial Platform for Chiral Responsive Optoelectronics

*Lei Kang, Shoufeng Lan, Yonghao Cui, Sean P. Rodrigues, Yongmin Liu, Douglas H. Werner, and Wenshan Cai**

Plasmonic metamaterials offer not only an unprecedented flexibility to control the flow of light in exotic, sometimes counterintuitive, manners,[1] but also an exciting opportunity to enable electrical and optical functions in a unified platform. This is because the metallic nanostructures that provide engineered plasmonic behavior for the metamaterial can also fulfill the conventional roles of metals for voltage bias, carrier injection, and current extraction. Without the need for elaborate modification, plasmonic systems with built-in electrical functions have demonstrated the potential of nanometallic structures for dual electrical and optical functionality. For example, the optical resonance in a bow-tie nanoantenna can remain essentially unaltered when the nanometallic parts are connected to external electrodes.[2] In addition, electrooptic plasmonic modulators utilize their metallic framework to control electroabsorptive or electrorefractive media embedded inside plasmonic resonators or waveguides.[3–6] Furthermore, nanostructured metals, including individual plasmonic resonators and photonic metamaterials, can facilitate electrically controlled nonlinear optical generation and emission.[7–9] Metamaterial-based photovoltaic cells were also reported,[10,11] where subwavelength hole-arrays were adopted to enhance the light trapping capability and simultaneously serve as electrodes for the collection of photocarriers. Other electrically active phenomena in plasmonics including the electrochemical charging effect of metallic particles,[12] the plasmon drag effect in metal films,[13] and the plasmoelectric potentials in metal nanostructures.[14] The utility of the aforementioned electro-active materials must unite with other genres of nano-optically engineered phenomena in order to realize the full potential of multifunctional platforms for light wave detection, modulation, and emission.

Chiral metamaterials are an important metamaterial species that give rise to enormously strong chiroptical responses. The past few years have witnessed an explosive development of chiral optical metamaterials that exhibit circular dichroism and optical rotation orders of magnitude larger than naturally occurring materials. Chirality, which is widely used as a powerful tool to identify compounds or measure concentrations in industrial and biological applications, is typically explored using transmitted light at normal incidence. Circularly polarized waves are characterized by the twisting of their electromagnetic field vectors as they travel; therefore a pronounced chiral response naturally requires structural variation of the meta-atom along the propagation direction. A wide range of 3D meta-atoms for artificially structured chiral materials have been explored at optical frequencies, including dual-layer twisted crosses,[15] rosettes,[16,17] split-rings,[18,19] gratings,[20] nano-arcs,[21] L-shapes,[22,23] coupled nanoparticles,[24] arrays of twisted nanorods of multiple stacks,[25] and 3D arrays of helices.[26,27] These structures, however, are not suited for electrically active applications because they typically consist of discrete, geometrically isolated metallic units, therefore prohibiting the control of chiral-selective optical responses by electrical means or the extraction of electrical information generated therein. To enable the application of electrical signals across a chiral structure, there is a keen need to construct a chiral optical metamaterial formed by topologically continuous plasmonic structures.

In this work we propose and experimentally demonstrate a novel metamaterial configuration that is composed of a pair of perforated films with angularly shifted elliptical holes. This metamaterial design gives rise to remarkably strong chiral-selective light-matter interactions in both the linear and nonlinear domains. With a deeply subwavelength thickness, the metamaterial exhibits a circular dichroism as large as 0.40 around the high frequency end of the near-infrared spectrum. This resonance behavior in turn leads to a pronounced contrast in the second-harmonic signal generated from the metamaterial under circularly polarized fundamental waves of opposite handedness. More importantly, the electrically connected metal parts that form the metamaterial facilitate the control and detection of chiroptical processes via electrical means. With such a unique feature, the metamaterial evolves into a self-contained optoelectronic platform with intrinsically embedded electrical and optical functions, thereby opening up the potential for electrooptic signal processing in the chiral

Dr. L. Kang, Dr. Y. Cui, S. P. Rodrigues, Prof. W. Cai
School of Materials Science and Engineering
Georgia Institute of Technology
Atlanta, GA 30332, USA
E-mail: wcai@gatech.edu
Dr. L. Kang, Prof. D. H. Werner
Department of Electrical Engineering and Center for Nanoscale Science
The Pennsylvania State University
University Park, PA 16802, USA
S. Lan, S. P. Rodrigues, Prof. W. Cai
School of Electrical and Computer Engineering
Georgia Institute of Technology
Atlanta, GA 30332, USA
Prof. Y. Liu
Department of Mechanical & Industrial Engineering
Northeastern University
Boston, MA 02115, USA

DOI: 10.1002/adma.201501930

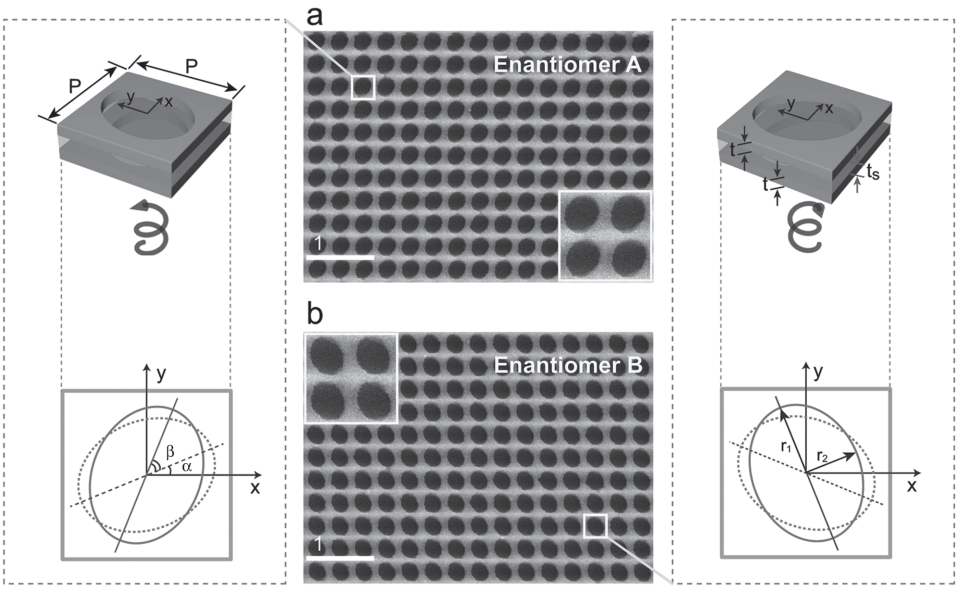

Figure 1. Chiral metamaterials of both enantiomers composed of a dual-layered continuous metallic pattern. a) SEM image of enantiomer A. The schematic on the left depicts two silver films ($t = 33$ nm) perforated by identical elliptical holes with angular offsets of $\alpha = 22.5°$ and $\beta = 45°$ from the *x*-axis, separated by a spin-on glass spacer ($t_s = 45$ nm). The dashed and solid ellipses indicate the lower and upper elliptical holes whose semi-major (r_1) and -minor (r_2) axes are 150 and 115 nm, respectively. The unit cell is arranged in a 2D square lattice with a lattice constant of 350 nm. b) SEM image and schematic of enantiomer B, which is mirror symmetric with respect to enantiomer A. Enlarged SEM images for both enantiomers are also presented.

optical regime. To demonstrate the platform potential in this regard, we explore the photoelectric current generated in the metamaterial under circularly polarized excitations, by means of the photon drag effect.

The chiral metamaterial used in our study is composed of a silver/glass/silver sandwich stack with the two metallic layers perforated by twisted-elliptical holes. The purposely introduced structural variation along the light propagation direction is essential to obtain a substantial chiral response from the transmitted waves. This design was inspired by a similar structure in search of chiral responses at terahertz frequencies.[28] **Figure 1** provides scanning electron microscope (SEM) images of the samples along with the corresponding schematic of the unit cells for each enantiomer, a term referring to objects of opposite handedness but identical scalar dimensions. The two enantiomers are mirror images of each other and are expected to exhibit complementary behaviors in terms of their chiral responses. Aligned electron-beam lithography is used to implement the design, which was optimized from full-wave simulations. The fabrication was achieved with a lateral alignment error of less than 10 nanometers. The metamaterial possesses a total thickness of ≈110 nm, which corresponds to only 1/7 of the targeted operating wavelength.

We first performed full-wave numerical simulations to evaluate the chiral responses of the two enantiomers in the linear optical regime. As illustrated in **Figure 2**a, a resonance dip in the transmission spectra for enantiomer A is observed at wavelengths of 820 and 880 nm, respectively, under right circularly polarized (RCP) and left circularly polarized (LCP) illumination. The power transmission coefficients T_{RR} (T_{LR}) is defined as the ratio of RCP (LCP) component of the transmitted power through the metamaterial to that of the RCP incidence, and a similar meaning applies to notation T_{LL} (T_{RL}). The cross conversion of circular polarization represented by T_{LR} and T_{RL} is less than 7% within the wavelength range of interest, which implies that the polarization state of the incidence is well preserved in the transmitted wave. Accordingly, two other characteristics of optical chirality, namely the linear polarization rotation angle $\theta = [\arg(t_{RR}) - \arg(t_{LL})]/2$, where $\arg(t_{RR})$ and $\arg(t_{LL})$ denote the phase of the complex transmission coefficients of RCP and LCP waves, and the ellipticity of the transmitted wave $\eta = \arctan[(T_{RR} - T_{LL})/(T_{RR} + T_{LL})]/2$, are calculated for enantiomer A and shown in Figure 2c. As a clear indication of the strong optical chirality, an optical activity of 25° (or $\approx 190°/\lambda$) is achieved around a wavelength of 850 nm. It is expected that enantiomer B precisely exhibits opposite chiral responses compared to enantiomer A, which is indeed confirmed in Figure 2b,d. To better illustrate the underlying physics at the chiral resonance, we show the distribution of the electric field cut at the middle of the two silver layers of enantiomer A in Figure 2e–h. An eigenmode resonance of the structure is identified at each of the resonance wavelengths under the corresponding circular polarization, as indicated by the hot spots related to the locally enhanced electric field. This circular-polarization-dependent field concentration leads to not only distinct features in the transmission spectra, but also increased chiral-selective efficiency for nonlinear light generation as seen in later experiments. Moreover, the resonance enhanced, asymmetric field distribution in the continuous metallic structure enables the direct momentum coupling of circularly polarized photons to free electrons, which enables a chiral-sensitive photon drag effect.

To characterize the linear chiral responses of the proposed metamaterial, we measured the transmittance spectra of both

Adv. Mater. **2015**,
DOI: 10.1002/adma.201501930

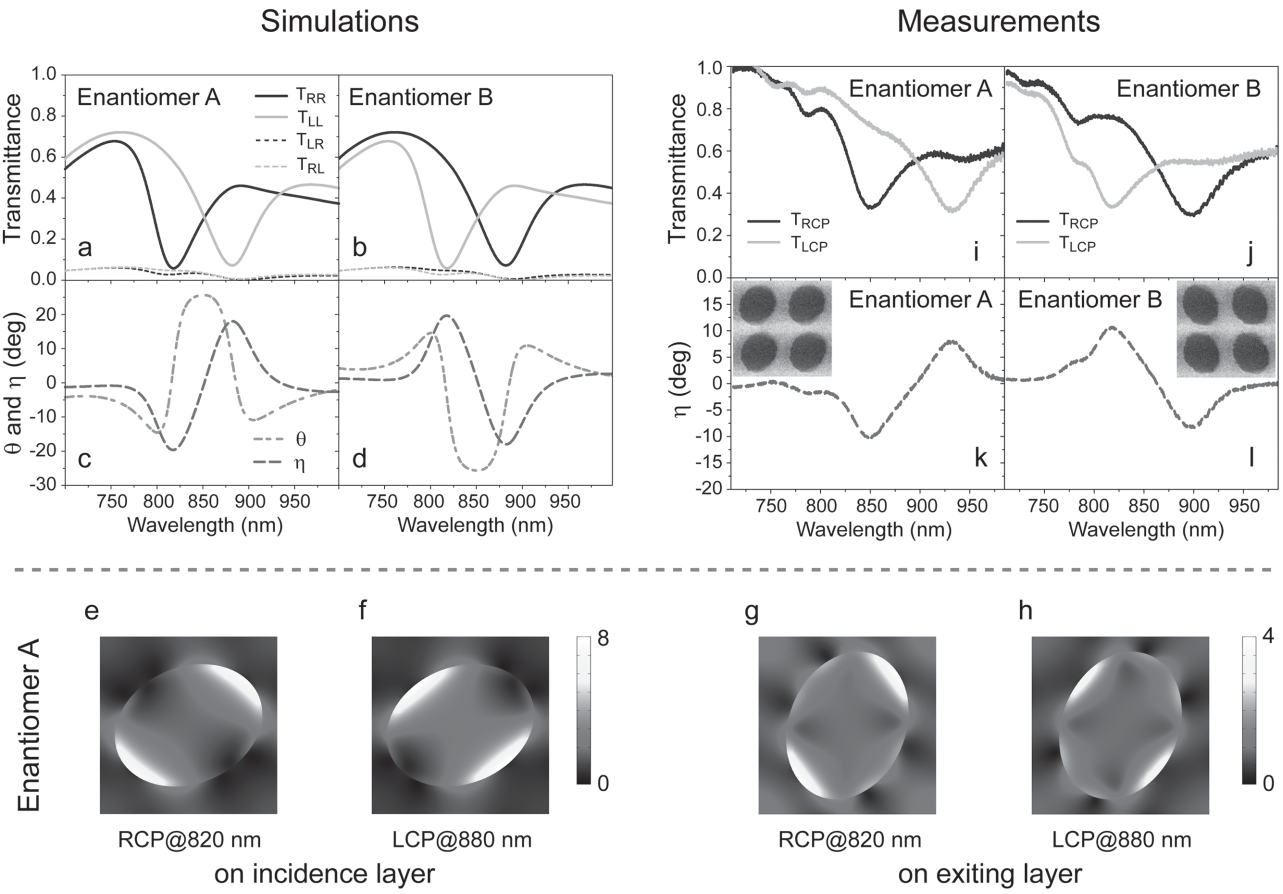

Figure 2. Simulated and measured linear chiral responses of both enantiomers. a,b) Transmittance spectra of enantiomer A and enantiomer B under LCP and RCP illumination. c,d) The polarization rotation angle (θ) of linearly polarized light and the ellipticity (η) of the transmitted wave for enantiomer A and enantiomer B, respectively. e–h) The magnitude of the electric field cut from the middle of the two silver layers ((e,f) incident layer and (g,h) exiting layer), when enantiomer A is excited at the resonance wavelength that corresponds to the given circular polarization. The electric field magnitude is normalized to that of the incident field. i,j) Measured transmittance spectra of enantiomer A and enantiomer B under RCP and LCP illumination. k,l) Ellipticity (η) of the transmitted wave from enantiomer A and enantiomer B, respectively. SEM images of the corresponding samples are shown in the insets.

enantiomers under the illumination of circularly polarized waves, using a homemade spectroscopy system designed for samples of small dimensions. The experimental results of the transmission normalized by that of an unpatterned substrate are illustrated in Figure 2i,j, where two distinct transmittance spectra for the two circular polarizations are observed for each of the enantiomers. The experimental data fits well with the numerical results presented in Figure 2a,b. A transmittance minimum for enantiomer A under RCP (LCP) illumination is observed around the resonance wavelength of 850 nm (930 nm), along with a corresponding circular dichroism $|T_{RCP} - T_{LCP}|$ of 0.40 (0.26). The enantiomer pair is expected to exhibit opposite spectra of the circular dichroism, as clearly evidenced from the experiment. Furthermore, in Figure 2k,l we plot the dispersion of the ellipticity (η) of the transmitted wave through the sample, which once again reveals the complementary behavior of the enantiomer pair and shows a good agreement between the measured and simulated data (Figure 2c,d). The remarkable linear chiral responses demonstrated here display the potential of the proposed metamaterial to interact with the circular polarized photons for chiral selective nonlinear optics and the photon drag effect.

The standard linear chiral properties of metamaterials may far exceed the properties of chiral materials found in nature, but are further succeeded by their nonlinear counterparts. In fact, second order nonlinear processes, such as second harmonic generation (SHG), are naturally suited for the study of chiral materials, because both the optical chirality and the susceptibility $\chi^{(2)}$ demand a lack of inversion symmetry in the structure. The second harmonic signal is further influenced by symmetry breaking at the interfaces of the metal-dielectric structures. Moreover, the light concentrating ability of the chiral metamaterial facilitates enhanced nonlinear light-matter interactions, thereby offering a valuable platform to study a wide range of chiral-selective nonlinear effects for imaging, sensing, and spectroscopic applications.[29–33] To investigate the disambiguation of the two enantiomers in the nonlinear regime, we excite the chiral metamaterial sample of both enantiomers with a circularly polarized ultrafast laser and characterize the generated nonlinear signals along the transmission direction.

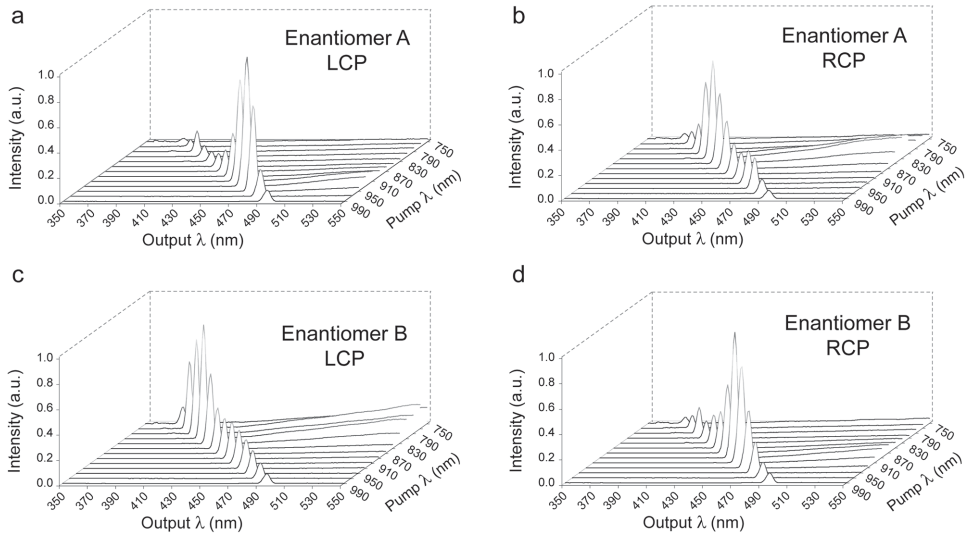

Figure 3. Chiral-selective nonlinear response of the chiral metamaterial under circularly polarized excitations. a,b) Experimentally collected nonlinear spectra of enantiomer A pumped by LCP and RCP light, respectively, for a series of excitation wavelengths at a constant intensity. c,d) Illustrations of the counterparts for enantiomer B.

Figure 3 shows the spectra of the nonlinear output emerging from the sample at a series of wavelengths under circularly polarized excitations. The intensity of the pump light is maintained at a constant level. At each excitation wavelength $\lambda\omega$, the output spectrum features an SHG peak at $\lambda\omega/2$, which is situated upon a weak, broadband background of multiphoton luminescence. Under the pump light of a given circular polarization, each of the enantiomer pair explicitly exhibits chiral-sensitive nonlinear signals. The SHG outcome reaches its pinnacle when the fundamental wavelength meets the respective resonance conditions in the linear regime. To better illustrate the correlation between the resonance behavior of SHG and the corresponding linear chiral responses, in **Figure 4** we generate the SHG excitation spectra by integrating the photon counts of the SHG peaks found in Figure 3. The connection between the resonances in the linear transmission behavior and the SHG efficiency is evident. For example, SHG output intensity from enantiomer A peaks at the fundamental wavelength of 830 and 930 nm, respectively, when pumped with RCP and LCP lights. These two values match well with the resonance wavelengths in the transmittance spectra (Figure 2i,j), as a transmission dip corresponds to an eigenmode with an enhanced local intensity of light (Figure 2e,f) that boosts the nonlinear optical generation. As a signature characteristic of SHG, the amount of the frequency doubled signal is expected to be quadratic to the intensity of the circularly polarized pump light. This is confirmed experimentally as seen in the double logarithmic plot in Figure 4c, which manifests the quadratic power dependence with very modest saturation behavior toward the high-intensity end. Note that spot size with a beam diameter of approximately 50 μm was fixed on the sample during the power dependence measurements, so an excitation power of 10 mW in Figure 4c implies a peak intensity of approximately 60 MW cm^{-2}.

Compared to most other optical metamaterials with drastic chiral responses collected from the transmitted light, a distinct feature of the current design is that it consists of geometrically continuous metallic films that facilitate electrooptic control schemes for information extraction. As an example to illustrate this capability, in the next section of the experimental study we investigate the photon drag effect (PDE) in our chiral metamaterial. The phenomenon of PDE is a direct consequence of the law of momentum conservation, where electrical signals arise from the momentum transfer from impinging photons to the free electrons in a conductor.[34] Recently, the PDE has been observed in a variety of plasmonic structures[35–38] and offers a new potential route to electrooptic information processing. The realization of the PDE typically requires oblique illumination or asymmetric plasmonic patterns in order to disrupt the centrosymmetry of the system and generate a net current flow. Photoinduced voltage in perforated metallic films was also observed under circularly polarized irradiation, where oblique incidence was again required to provide the translational momentum for the photon–electron coupling.[39,40]

The chiral metamaterial used in this work offers the intrinsic absence of inversion symmetry that enables the transfer of angular momentum of incoming photons to the free electrons in the continuous metallic film, even under normal incidence. The experimental configuration is illustrated in **Figure 5**a, where photoinduced current flowing through the metamaterial pattern is monitored under various illumination conditions. Figure 5b depicts the light-induced current in the two enantiomers under circularly polarized excitations, where the wavelength of the constant-intensity pump source is swept across the operating band of the chiral metamaterial. The magnitude of the generated electrical signal is clearly correlated to the chiroptical resonances observed earlier. For example, the photoinduced current in enantiomer B reaches its maximum values when excited around the wavelength of 810 and 890 nm, respectively, for the two circularly polarized irradiations. More importantly, the photoinduced currents flow along opposite directions for the two enantiomers. This reveals the chirality-sensitive coupling of circularly polarized photons to the nanometallic

Adv. Mater. **2015**,
DOI: 10.1002/adma.201501930

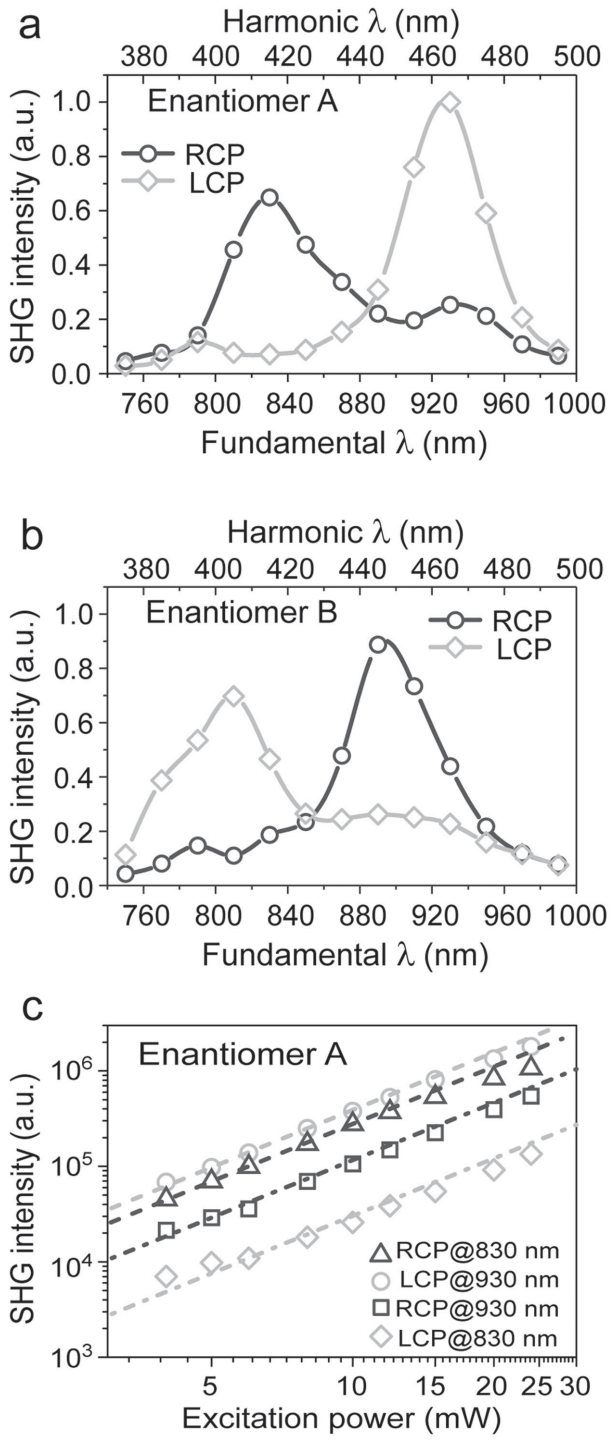

Figure 4. Resonance-enhanced, chirally sensitive second harmonic generation from the metamaterial. a) Frequency-doubled output from enantiomer A under circularly polarized excitations of opposite handedness. The empty symbols represent the measured results and the solid curves are to guide the eye. Similarly, the SHG excitation spectra for enantiomer B are plotted in (b). c) Intensity dependent SHG from circularly polarized fundamental waves incident on enantiomer A. Data were collected at the two resonance wavelengths as indicated in (a). The dashed and dashed-dotted lines are linear curves with slopes of 2.0 in the log–log plot demonstrating the quadratic relation.

system originating from the intrinsic enantio-selectivity in the chiral metamaterial. While a number of physical processes can lead to photon-induced current or voltage, we attribute the observed electrical signals to the PDE and rule out the possibilities of photoconductive, pyroelectric, and thermoelectric effects with the following reasoning. Observation of the photoconductive effect requires a bias voltage that is not presented in our experiments. Moreover, a control experiment confirms that no detectable current can be found from an unpatterned metal film under a similar experimental condition. We further rule out the pyroelectric effect since the induced current signal remains stable when the circularly polarized excitation is kept constant. Furthermore, we exclude the thermoelectric effect because the sample is illuminated in a symmetric manner without an asymmetric temperature gradient across the metal. A consistent microscopic theory of the PDE effects with circularly polarized excitation of chiral metamaterials is desired, but is beyond the scope of this work. In the photoinduced current measurements a lock-in amplification setup is employed to measure the time-integrated response from an ultrafast laser. The detector is locked to an optical chopper (≈325 Hz) through which the input laser-signal passes. The photoinduced current signals are evaluated as a time–averaged current flowing through the metamaterial pattern.

A detailed comparison between the excitation spectra of the PDE in Figure 5b and those of SHG in Figure 4a,b shows that, at excitation wavelengths around the resonances, the chiral-selectivity of SHG is more significant than that of the PDE signal. For example, when enantiomer A is pumped at a wavelength of 830 nm, the SHG signal with RCP excitation is 9 times as large as that of the LCP generated harmonic output, while this contrast is reduced to a factor of 2.6 for the photon-induced current. This difference in the level of chiral-selectivity is likely due to the distinct intensity dependences of the two physical processes. While SHG is known to be quadratic to the pump intensity, the induced current originating from the PDE is linearly proportional to the illumination intensity.[13] This linear dependence of the photoinduced current on the excitation intensity is experimentally confirmed for a representative illumination condition, as shown in Figure 5c.

In summary, we demonstrate a photonic metamaterial with enormously strong chiral responses in both the linear and the nonlinear optical regimes. The meta-enantiomer pair exhibits complementary chiroptical effects, including a circular dichroism of 0.4 in the transmission spectrum and a factor of 9 in terms of the contrast in the second harmonic generation. More importantly, the topologically continuous metallic structure in the metamaterial facilitates electrooptic control and signal generation, thereby forming a self-contained platform with dual electrical and optical functions. Under circularly polarized excitations at normal incidence, the metamaterial produces light-induced electrical signals arising from the photon drag effect, which, like the harmonic generation of light, demonstrates chiral-selective behavior correlated to the chiral resonances in the linear domain. With the combined study of harmonic generation and photon dragging in the metamaterial, both the energy and momentum of circularly polarized photons are exploited in a unified manner. The multifunctional chiral metamaterial demonstrated in this work may

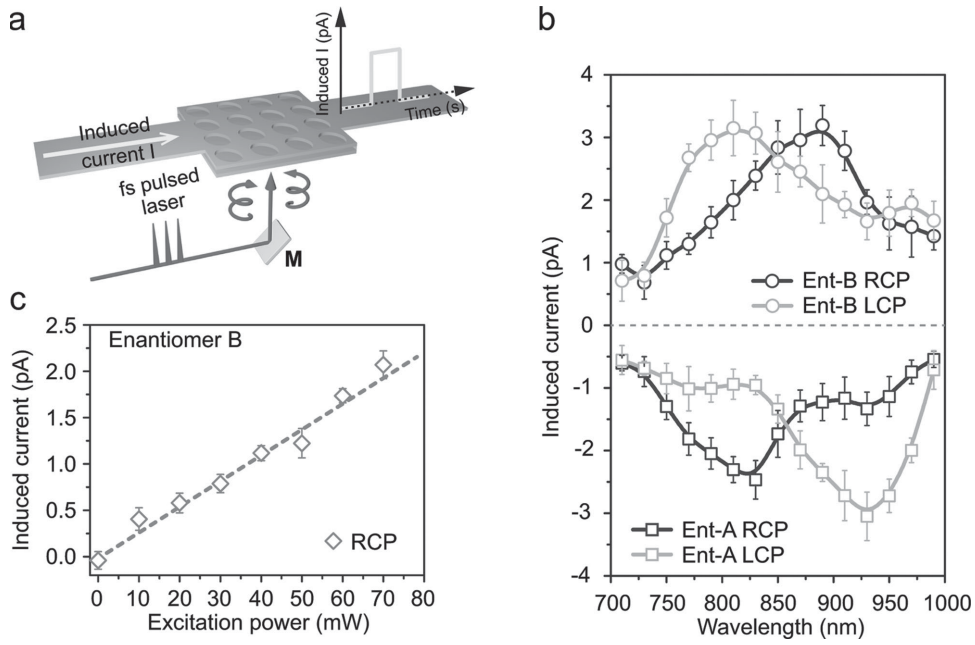

Figure 5. Chiral-selective photon drag effect in the chiral metamaterial. a) Schematic of the optically induced current generated from incident circularly polarized lights. Under illumination of pulsed lasers, other nonlinear signals would also arise from the structure. b) Induced electric currents flowing through enantiomers A and B as a function of wavelength of circularly polarized pump lights at a constant intensity. Photoinduced currents of opposite directions are generated in the enantiomer pair. The empty symbols represent the measured results and the solid curves are to guide the eye. c) Dependence of the photo drag signal on the pump intensity for RCP illumination at the resonant wavelength of 890 nm. The dashed line represents a least-square linear fit to the experimental data. All error bars represent standard deviations from five measurements.

promise diverse applications in biochemical analysis and information technology where chiroptical information is generated, processed, and utilized.

Acknowledgements

L.K., S.L., and Y.C. contributed equally to this work. This work was performed in part at the Georgia Tech Institute for Electronics and Nanotechnology, a member of the National Nanotechnology Infrastructure Network, which is supported by the National Science Foundation. W.C. acknowledges the start-up fund from the Georgia Institute of Technology and the generous gift by OPE LLC in support of the scientific research in the Cai Lab. S.P.R. acknowledges the support of the National Science Foundation Graduate Research Fellowship under Grant No. DGE-1148903.

Received: April 22, 2015
Revised: May 15, 2015
Published online:

[1] W. Cai, V. M. Shalaev, *Optical Metamaterials: Fundamentals and Applications*, Springer, New York **2010**.
[2] J. C. Prangsma, J. Kern, A. G. Knapp, S. Grossmann, M. Emmerling, M. Kamp, B. Hecht, *Nano Lett.* **2012**, *12*, 3915.
[3] M. J. Dicken, L. A. Sweatlock, D. Pacifici, H. J. Lezec, K. Bhattacharya, H. A. Atwater, *Nano Lett.* **2008**, *8*, 4048.
[4] J. A. Dionne, K. Diest, L. A. Sweatlock, H. A. Atwater, *Nano Lett.* **2009**, *9*, 897.
[5] W. S. Cai, J. S. White, M. L. Brongersma, *Nano Lett.* **2009**, *9*, 4403.
[6] A. Melikyan, L. Alloatti, A. Muslija, D. Hillerkuss, P. C. Schindler, J. Li, R. Palmer, D. Korn, S. Muehlbrandt, D. Van Thourhout, B. Chen, R. Dinu, M. Sommer, C. Koos, M. Kohl, W. Freude, J. Leuthold, *Nat. Photonics* **2014**, *8*, 229.
[7] Y. C. Jun, K. C. Y. Huang, M. L. Brongersma, *Nat. Commun.* **2011**, *2*, 283.
[8] W. S. Cai, A. P. Vasudev, M. L. Brongersma, *Science* **2011**, *333*, 1720.
[9] L. Kang, Y. H. Cui, S. F. Lan, S. P. Rodrigues, M. L. Brongersma, W. S. Cai, *Nat. Commun.* **2014**, *5*, 4680.
[10] H. J. Park, T. Xu, J. Y. Lee, A. Ledbetter, L. J. Guo, *ACS Nano* **2011**, *5*, 7055.
[11] S. Y. Chou, W. Ding, *Opt. Express* **2013**, *21*, A60.
[12] C. Novo, A. M. Funston, A. K. Gooding, P. Mulvaney, *J. Am. Chem. Soc.* **2009**, *131*, 14664.
[13] N. Noginova, A. V. Yakim, J. Soimo, L. Gu, M. A. Noginov, *Phys. Rev. B* **2011**, *84*, 035447.
[14] M. T. Sheldon, J. van de Groep, A. M. Brown, A. Polman, H. A. Atwater, *Science* **2014**, *346*, 828.
[15] M. Decker, M. Ruther, C. E. Kriegler, J. Zhou, C. M. Soukoulis, S. Linden, M. Wegener, *Opt. Lett.* **2009**, *34*, 2501.
[16] E. Plum, V. A. Fedotov, A. S. Schwanecke, N. I. Zheludev, Y. Chen, *Appl. Phys. Lett.* **2007**, *90*, 223113.
[17] D. H. Kwon, P. L. Werner, D. H. Werner, *Opt. Express* **2008**, *16*, 11802.
[18] M. Decker, R. Zhao, C. M. Soukoulis, S. Linden, M. Wegener, *Opt. Lett.* **2010**, *35*, 1593.
[19] N. Liu, H. Liu, S. N. Zhu, H. Giessen, *Nat. Photonics* **2009**, *3*, 157.
[20] W. S. Gao, H. M. Leung, Y. H. Li, H. Chen, W. Y. Tam, *J. Optics* **2011**, *13*, 115101.
[21] Y. H. Cui, L. Kang, S. F. Lan, S. Rodrigues, W. S. Cai, *Nano Lett.* **2014**, *14*, 1021.

[22] C. Helgert, E. Pshenay-Severin, M. Falkner, C. Menzel, C. Rockstuhl, E. B. Kley, A. Tunnermann, F. Lederer, T. Pertsch, *Nano Lett.* **2011**, *11*, 4400.
[23] K. Dietrich, D. Lehr, C. Helgert, A. Tunnermann, E. B. Kley, *Adv. Mater.* **2012**, *24*, Op321.
[24] M. Hentschel, L. Wu, M. Schaferling, P. Bai, E. P. Li, H. Giessen, *ACS Nano* **2012**, *6*, 10355.
[25] Y. Zhao, M. A. Belkin, A. Alu, *Nat. Commun.* **2012**, *3*, 870.
[26] J. K. Gansel, M. Thiel, M. S. Rill, M. Decker, K. Bade, V. Saile, G. von Freymann, S. Linden, M. Wegener, *Science* **2009**, *325*, 1513.
[27] M. Esposito, V. Tasco, F. Todisco, M. Cuscuna, A. Benedetti, D. Sanvitto, A. Passaseo, *Nat. Commun.* **2015**, *6*, 6484.
[28] S. X. Wang, F. Garet, E. Lheurette, M. Astic, J. L. Coutaz, D. Lippens, *APL Mater.* **2013**, *1*, 032116.
[29] V. K. Valev, A. V. Silhanek, N. Verellen, W. Gillijns, P. Van Dorpe, O. A. Aktsipetrov, G. A. E. Vandenbosch, V. V. Moshchalkov, T. Verbiest, *Phys. Rev. Lett.* **2010**, *104*, 127401.
[30] M. J. Huttunen, G. Bautista, M. Decker, S. Linden, M. Wegener, M. Kauranen, *Opt. Mater. Express* **2011**, *1*, 46.
[31] V. K. Valev, J. J. Baumberg, C. Sibilia, T. Verbiest, *Adv. Mater.* **2013**, *25*, 2517.
[32] S. P. Rodrigues, S. F. Lan, L. Kang, Y. H. Cui, W. S. Cai, *Adv. Mater.* **2014**, *26*, 6157.
[33] S. P. Rodrigues, Y. H. Cui, S. F. Lan, L. Kang, W. S. Cai, *Adv. Mater.* **2015**, *27*, 1124.
[34] A. F. Gibson, M. F. Kimmitt, A. C. Walker, *Appl. Phys. Lett.* **1970**, *17*, 75.
[35] A. S. Vengurlekar, T. Ishihara, *Appl. Phys. Lett.* **2005**, *87*, 091118.
[36] T. Hatano, B. Nishikawa, M. Iwanaga, T. Ishihara, *Opt. Express* **2008**, *16*, 8236.
[37] A. English, C. W. Cheng, L. Lowe, M. H. Shih, W. Kuang, *Appl. Phys. Lett.* **2011**, *98*, 191113.
[38] N. Noginova, V. Rono, F. J. Bezares, J. D. Caldwell, *New J. Phys.* **2013**, *15*, 113061.
[39] T. Hatano, T. Ishihara, S. G. Tikhodeev, N. A. Gippius, *Phys. Rev. Lett.* **2009**, *103*, 103906.
[40] M. Akbari, M. Onoda, T. Ishihara, *Opt. Express* **2015**, *23*, 823.